# 3D numerical prediction of residual stresses in turning of 15-5PH

Alexandre Mondelin, Frederic Valiorgue, Joel Rech, Michel Coret, Eric Feulvarch

# 3D numerical prediction of residual stresses in turning of 15-5PH

Alexandre Mondelin[1,2,a], Frédéric Valiorgue[1,b] ,Joël Rech[1,c] , Michel Coret[2,d], Eric Feulvarch[1,e]

[1]University of Lyon, Ecole Nationale d'Ingénieurs de Saint Etienne, Laboratoire de Tribologie et Dynamique des Systèmes, UMR CNRS 5513, 58 rue Jean Parot, 42023 Saint-Etienne, France

[2]University of Lyon, Institut National des Sciences Appliquées de Lyon, LaMCoS, UMR CNRS 5259, 27 avenue Jean Capelle, 69621 Villeurbanne Cedex, France

[a]alexandre.mondelin@enise.fr, [b]frederic.valiorgue@enise.fr, [c]joel.rech@enise.fr, [d]michel.coret@insa-lyon.fr, [e]eric.feulvarch@enise.fr

**Keywords:** Hybrid method; Residual stresses; Turning; 3D numerical modeling; Surface integrity.

**Abstract.** This study presents the development of a numerical model for the prediction of residual stresses induced in finish turning of a 15-5PH martensitic stainless steel. This methodology uses a hybrid approach combining experimental results (friction and orthogonal friction tests) with a numerical model. The numerical model simulates the residual stresses generation by applying cyclic equivalent thermo-mechanical loads onto the machined surface without modeling the chip removal process. The three-dimensional approach enables to study the influence of the turning passes interactions. It has been shown numerically that the periodicity of loading leads to a significant heterogeneity of material solicitations. Moreover, overlapping of passes accentuates these effects. So, the model highlights the necessity of a multi-passes simulation to reach a constant evolution of residual stresses along the feed direction. In addition, experimental measurements obtained by X-Ray diffraction have been compared with numerical results to validate the model.

## 1. Introduction

The 15-5 PH stainless steel is a low-carbon martensite stainless steel containing approximately 3 wt% Cu. It is strengthened by the precipitation of highly dispersed copper particles in the martensite matrix. Several studies have been reported in the literature concerning the microstructural characterization [1] and mechanical behavior of PH stainless steels [2, 3].

Precipitated hardening (PH) stainless steels show excellent mechanical properties, low distortion and excellent weldability and good corrosion resistance. That is why they are used in aerospace and nuclear industries. Predicting the fatigue resistance of mechanical parts is crucial for these industries. Fatigue is significantly affected by several parameters such as surface roughness, residual stress and microstructure, which are commonly summarized by the term "surface integrity" [4]. Surface integrity depends on the thermo-mechanical loadings induced by all the previous manufacturing operations, even if the last operation has a major responsibility. Among the finishing operations applied on critical parts, longitudinal finish turning is widely applied. This paper focuses on the modeling of residual stresses generated by finish longitudinal turning of the 15-5PH martensitic stainless steel.

Experimental studies were performed to quantify the effects of cutting parameters on surface integrity [5]. In parallel, various models have been developed. Historically, analytical models were the most popular [6]. Several contributions have improved its work [7, 8]. Such models enable very fast calculations. They facilitate a good understanding of phenomena involved in residual stress generation. Unfortunately, severe assumptions do not enable to provide quantitative results. Different numerical models have also been developed. [9, 10] have used a numerical Lagrangian formulation of the material removal process. However, such models meet two main difficulties: the separation criterion around the cutting edge radius [11, 12] and the modeling of friction [13]. Moreover lagrangian models necessitate large calculation duration. Some models, similar as the one

proposed by [14], use an Arbitrary Lagrangian Eulerian (A.L.E) formulation providing rapid results. These works use an explicit integration method.

An alternative approach proposed by [15] consists in modeling residual stress generation by removing the chip formation and by replacing it by equivalent thermo-mechanical loadings (Fig. 1). These equivalent loadings are moved onto the machined surface with a velocity equal to the cutting speed. Such a model uses an implicit formulation. After the cooling phase, this model enables to predict residual stresses. The shape and the intensity of these equivalent thermo-mechanical loadings are estimated by means of preliminary experimental tests: friction tests and orthogonal cutting tests. However such models only consider orthogonal cutting configuration (2D) which is not relevant to simulate accurately a common longitudinal turning operation. Indeed, during a turning operation, the cutting tool makes a large number of revolutions around the workpiece (Fig. 2). The cutting tool modifies the residual stress state obtained during the previous revolution. When machining with low feed and large nose radius, which is typical in finish turning, it can be assumed that several revolutions are necessary to reach a steady state. Hence, 2D models are interesting to understand the mechanisms involved during the surface integrity generation, but they are not able to provide quantitative data comparable with practical longitudinal turning operations.

Based on this statement, some researchers started 3D simulations. [16] proposed to combine two Lagrangian plane models: an orthogonal cutting simulation containing the cutting direction and an indentation-like simulation of a corner radius into the machined surface (containing the feed direction). A more recent model, proposed by [17], uses a Lagrangian formulation (software DEFORM 3D) to predict residual stress induced during cutting. This work is an important step forward. Nevertheless, the limitation of this Lagrangian formulation has already been mentioned previously and this code does not consider any variation of the friction coefficient along the contact. Finally the calculation time is too long to be compatible with an industrial exploitation.

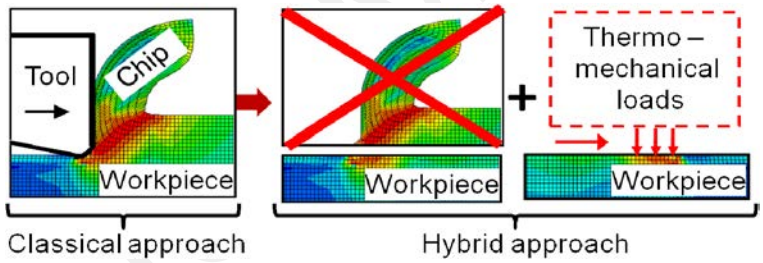


Fig. 1: Principle of the hybrid model.

Hence, the main objective of this paper is to present a generalized 3D model of residual stresses prediction, accurately described in [18], based on the equivalent thermo-mechanical approach proposed by [15] and adapted to the 15-5PH martensitic stainless steel. Numerical results will be compared with experimental measurements obtained by X-ray diffraction.

## 2. Numerical model design

The model aims at simulating residual stress generation on a cylinder machined by a finish longitudinal turning operation (Fig. 2).

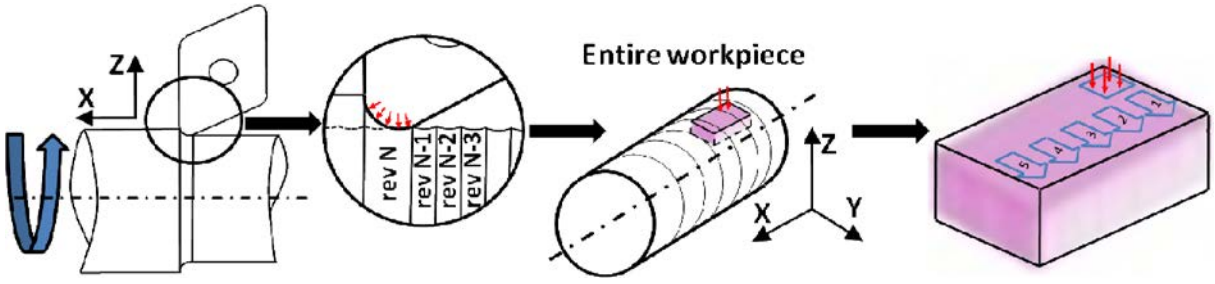


Fig. 2: 3D hybrid modeling strategy.

As mentioned previously, the proposed model does not consider the chip removal mechanisms. The machined part is modeled as a cylinder (Fig. 2). Moreover the cutting conditions are constant all along the surface, so it is possible to model only a small volume of the cylinder. Finally, if the diameter of the cylinder is large, the machined surface can be considered as flat. Hence, it becomes possible to model the residual stress generation in finish longitudinal turning by means of a parallelepiped (Fig. 2). The dimensions of the parallelepiped (1.5 mm x 2.3 mm x 0.8 mm) enable to simulate several turning revolutions. Five sides of this parallelepiped need to be in contact with the rest of the workmaterial. A large border of a perfectly elastic material (to reduce calculation duration) is positioned around the central parallelepiped. So, difficulties linked with boundaries effects are minimized and the real material stiffness is simulated. Heat exchanges are enabled between the mesh body, the rest of the workmaterial and the ambient. As presented in Fig. 3, a quadrangle linear mesh is applied and its size has been optimized in order to minimize calculation duration without disturbing the results accuracy. A fine mesh is necessary on the machined surface (0.003mm, 0,4mm, 0.0125mm), where the thermo-mechanical loadings are applied leading to strong gradient. On the contrary, larger meshes are used below the surface.

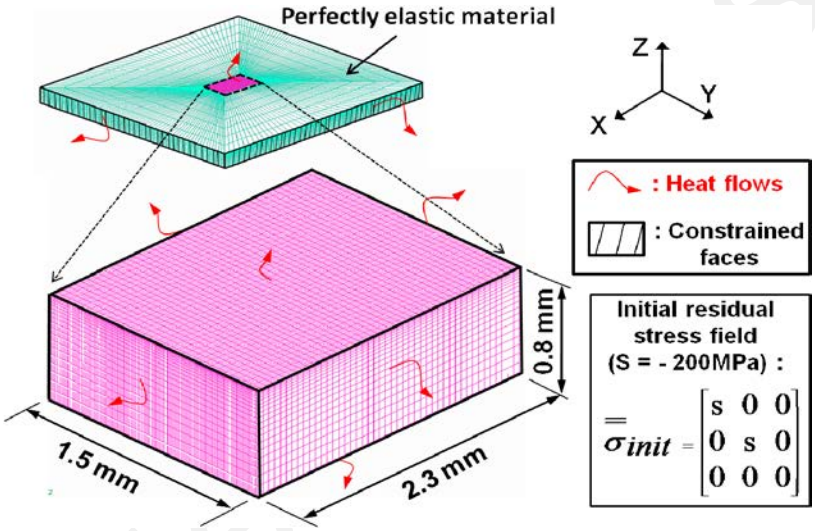


Fig. 3: 3D model geometrical parameters.

**2.1 Technological parameters.** The cutting tool is a TiCN-$Al_2O_3$ coated carbide insert: DNMG 150612. Reference cutting conditions have been chosen for the study. The cutting speed $V_c$ is 150m.min$^{-1}$. The feed rate *f is* 0.18mm.rev$^{-1}$ and the depth of cut $a_p$ is 0.6mm.

The workmaterial is a 15-5PH martensitic stainless steel in precipitation-hardened condition H1025 (40 HRC). It is not considered as free of residual stresses before the turning operation. X-ray diffraction measurements have shown an initial residual stress field of -200MPa in both the axial and tangential directions at the machining depth. The turning diameter is 175mm.

**2.2 Workmaterial mechanical and thermal properties.** The 15-5PH stainless steel properties have been extracted from [3] who provides flow stress curves and thermo-mechanical properties from 20°C to 850°C. So, a thermo-elasto-plastic behavior with an isotropic hardening is modeled. An initial residual stress field, corresponding to the measured one, has been induced in the model (Fig. 3).

Contrary to austenitic stainless steel, a phase transformation could occur during the heating of a martensitic stainless steel. [3] shows that the austenitic phase transformation starts at $AC_1$=665°C at a heating rate of 2°C.s$^{-1}$. The numerical model doesn't take into account phase transformations. Soft cutting and lubrication conditions have been chosen in order to avoid material change of phase (austenitic transformation) during the machining. Results of numerical simulation predict a maximum temperature of 560°C during turning. This temperature is below the austenitic start temperature and can confirm the assumption of not considering change of phase.

**2.3 3D Thermo-mechanical loadings shapes.** The model is based on the application of 3D equivalent thermo-mechanical loadings simulating the influence of the primary and of the third shear zone (Fig. 4). The section A considers phenomena in the cutting plane, whereas section B considers phenomena in the feed plane.

**Modeling in section A.** The shape of the thermo-mechanical loadings are inspired by the previous work of [15]. The quantification of the intensity of the loadings will be discussed later in the paper.

The primary shear zone (PSZ) is assumed as having a pure thermal influence. Its mechanical influence onto the final workpiece surface (elastic deformations) is neglected. In the PSZ, the heat flux density is assumed as being homogeneous. The width of the heat flux is assumed as being equal to the average chip thickness β.

The third shear zone (TSZ) is considered as having a thermal and a mechanical influence. The mechanical pressure is assumed having a parabolic shape. A friction coefficient, depending on the sliding velocity [19], is used in this zone. As a consequence, friction induces a parabolic shear load.

Additionally friction induces a heat flux at the interface. Heat is transmitted to the cutting tool and to the machined surface. The heat partition coefficient also depends on the sliding velocity [19].

**Modeling in section B.** It is necessary to distinguish two zones (Fig. 4):

- a zone, where the tool is directly in contact with the machined surface (Zone ②, Section B).
- a zone where the cutting tool is not in contact with the future machined surface (Zone ①, Section B). It is only in contact with the "section to be removed during the next revolution". The influence of the cutting tool is indirect.

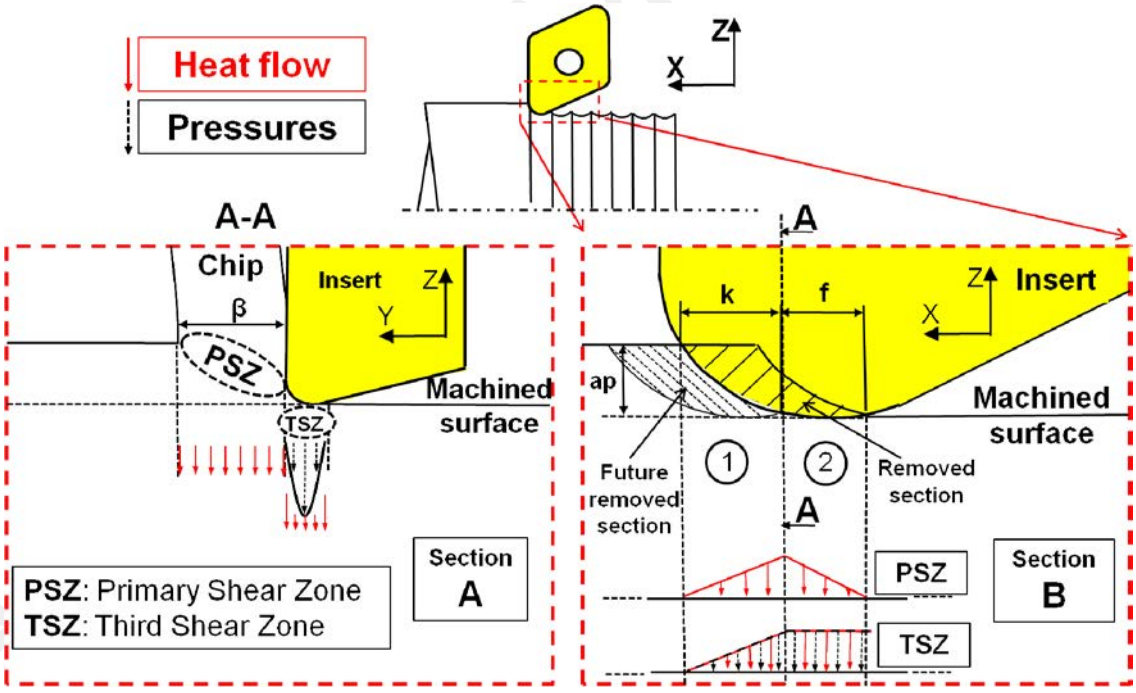


Fig. 4: Thermo-mechanical loadings at the 'tool – machined surface' interface.

In zone ② (=direct contact between the tool and the final machined surface):

- in the PSZ, the intensity of heat flux is assumed to depend on the radial uncut chip thickness. So, a triangular shape of load is used.
- in the TSZ, the intensity of the thermo-mechanical loads is supposed to be constant along the cutting edge. Homogeneous loads are applied.

In zone ① (=indirect influence of the cutting tool on the final machined surface), loads' intensity is assumed to depend on the thickness of the intercalated future removed chip section. Consequently, triangular shape is used for thermo-mechanical loads.

**2.4 Estimation of thermo-mechanical load intensity.** The quantification of the intensity of each thermo-mechanical loading is made by means of experimental elementary tests as described by [15]:

- Orthogonal cutting tests
- Friction tests

**Friction tests.** Friction tests are performed on a dedicated tribometer [19]. This experimental set-up, associated with a numerical treatment provides the evolution of friction coefficient and heat partition coefficient (Fig. 5). The case of a TiCN-$Al_2O_3$ coated carbide pin against a 15-5PH stainless steel has not been characterized at the moment. A friction model describing the behavior of a TiN coated carbide pin against a 15-5PH stainless steel has been used [20]. This model shows that friction coefficient ($\mu_{adh}$) and heat partition coefficient ($\Lambda_3$) depend mainly on sliding speeds (Eq. 1, Eq. 2, Eq. 3).

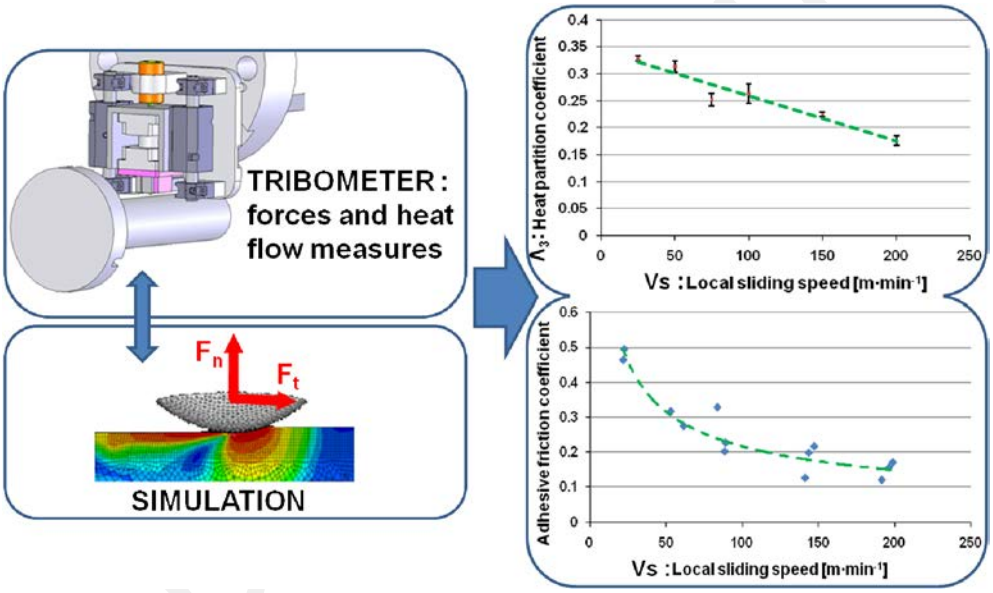


Fig. 5: Identification of friction coefficient and heat partition coefficient versus sliding velocity.

$$\mu_{adh}=2.63Vs^{-0.54}. \quad (1)$$

with $20\ m{\cdot}min^{-1} < Vs$ (local sliding speed) $< 200\ m{\cdot}min^{-1}$.

$$\mu_{adh}=0.15. \quad (2)$$

with $Vs > 200\ m{\cdot}min^{-1}$.

$$\Lambda_3=-0.0008Vs + 0.34. \quad (3)$$

**Orthogonal cutting tests.** Orthogonal cutting tests are performed in order to obtain (Fig. 6):

- the average chip thickness $\beta$,
- the 'tool-machined surface' contact length α (=contact length on the flank face)
- the macroscopic cutting force $F_c$,
- the macroscopic feed force $F_f$,

Based on these measurements, it is possible to estimate local cutting forces supported by the second and third shear zones using the methodology developed by [15].

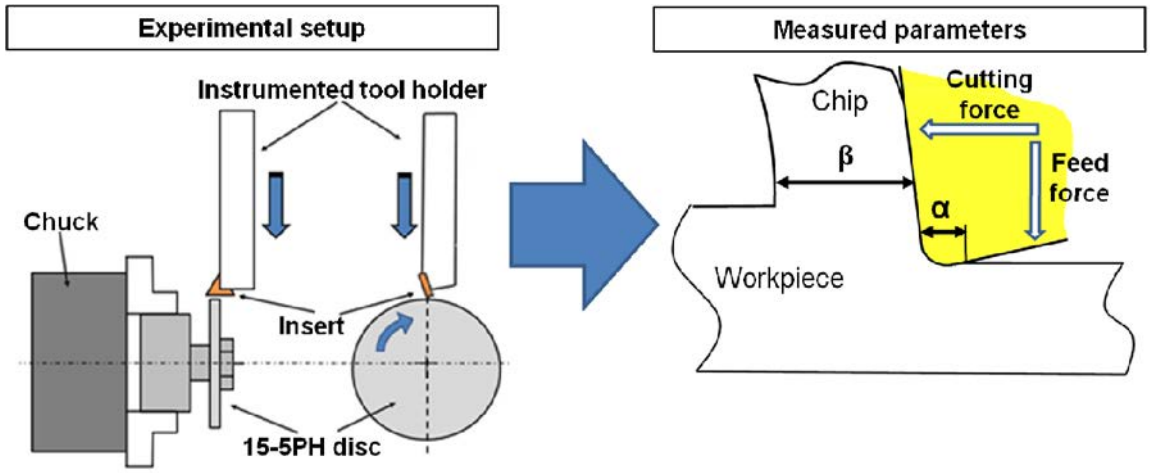


Fig. 6: Orthogonal cutting tests and investigated parameters angular surface.

**2.5 Application of the equivalent thermo-mechanical loadings on the 3D model.** A part of the workpiece is modeled as a parallelepiped. Thermo-mechanical loads are applied on a rectangular surface. These loadings are moved in the Y direction (cutting direction) with a velocity equal to the cutting speed (Fig. 7) up to cross the parallelepiped. Then a cooling period is necessary to simulate the movement of the cutting tool around the workpiece. Its value depends on the diameter of the workpiece $D$ and on the cutting speed $V_c$.

A second movement of the thermo-mechanical loads is simulated (Fig. 7b). The second movement is shifted in the direction X (feed direction) in order to simulate the feed per revolution of the cutting tool. Due to the fact that the width of the loaded zone $w$ is larger than the feed $f$, the thermo-mechanical load affects a part of the surface which has already been affected during the previous revolution (Fig. 7b). Then the simulation goes on with a second cooling phase and a third application of the thermo-mechanical loadings, etc…

In the present work, five revolutions are simulated since it will be shown later that it is sufficient to reach a steady state. At the end of the simulation, the material is cooled down to room temperature and the residual stresses are evaluated.

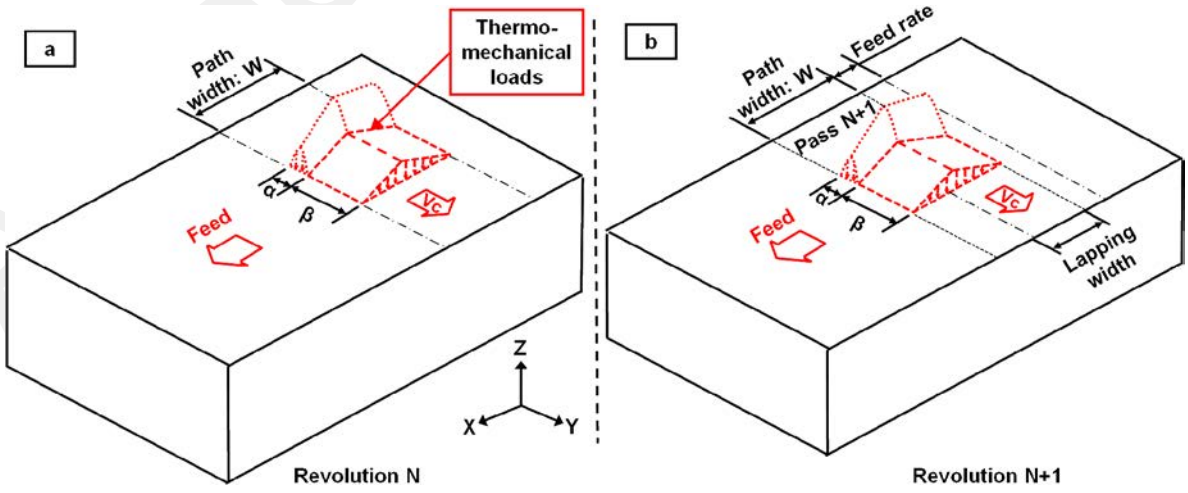


Fig. 7: 3D simulation strategy

## 3. Numerical results

The model has been applied to simulate the finish turning of a 15-5PH stainless steel with a TiCN-$Al_2O_3$ coated carbide tool under the following conditions:

- Cutting speed, Vc = 150 $m.min^{-1}$
- Feed, f : 0.18 $mm.rev^{-1}$
- Depth of cut, ap 0.6mm
- Lubricated condition (emulsion flow, h=0.1 $W.mm^{-2}.K^{-1}$ [21])

**3.1 General observations.** Fig. 8 presents the residual stress $\sigma_{xx}$ and $\sigma_{yy}$ along the "measurement line" at the surface of the meshed body. This line crosses the parallelepiped in its center in order to be far from its extremity. The direction Y is parallel to the cutting speed, whereas the direction X is parallel to the feed.

Fig. 8 presents the residual stress state after each revolution from the 1st to 7th. It reveals that the residual stress state induced after seven revolutions is not homogeneous nor in the Y direction nor in the X direction. Residual stresses along the measurement line are periodic. The period corresponds to the feed *f*. Fig. 8 also shows that, at least, three revolutions are necessary to obtain a steady state with such cutting conditions. By observing the residual stress state obtained after a revolution, it is observable that the curves are modified by the following revolutions. The periodic variation of residual stresses and the interaction between each path are two key results showing the limitations of 2D models which are not able to highlight such phenomena.

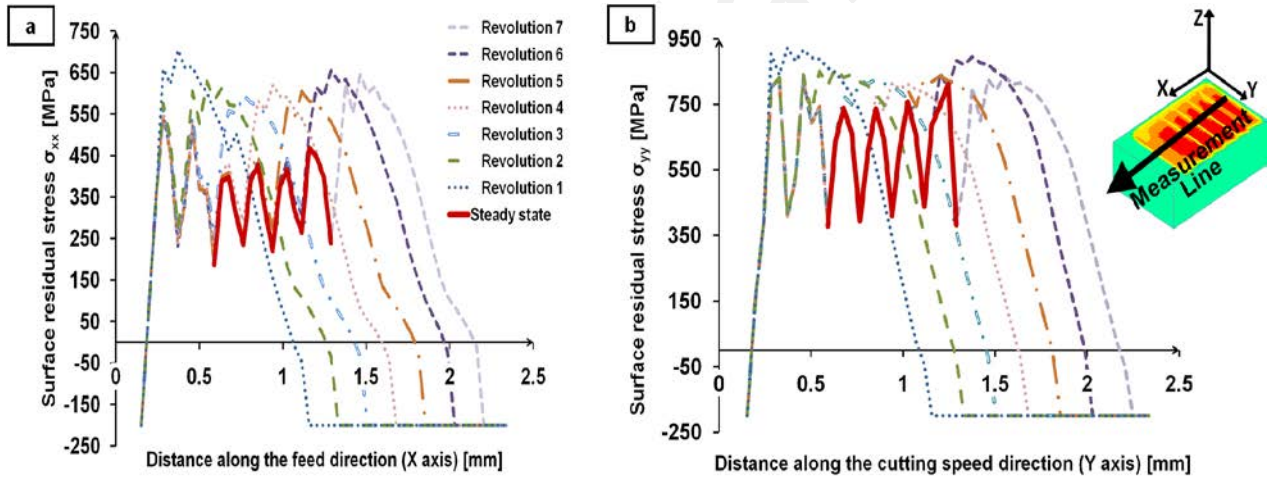


Fig. 8: Evolution of residual stresses on the surface along a measurement line for seven revolutions: (a) along the feed direction=X axis; (b) along the cutting speed direction =Y axis.

When analyzing residual stresses below the surface (residual stress profiles) and comparing it with experimental results, it is difficult to take into account the stress periodic variations along the feed direction. Hence it has been decided to calculate and consider the average value in the steady state.

Fig. 9 shows the averaged values calculated for each depth. It appears that tensile residual stresses are obtained in the external layer. Surface residual stress is 500 MPa in the feed direction ($\sigma_{xx}$) and 572 MPa in the cutting direction ($\sigma_{yy}$).A peak of compression (-320MPa) is obtained at a distance around 0.04 mm from the surface. The affected depth is about 0.07mm.

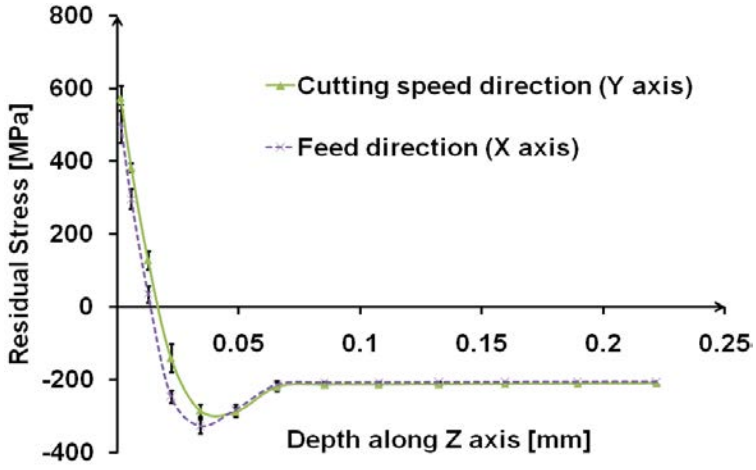


Fig. 9: Calculated residual stresses profiles in the X and Y direction.

## 4. Experimental characterization

**4.1 Measuring set-up.** Numerical results will now be compared with experimental measurements obtained by X-ray diffraction. Cylindrical parts have been turned with the same cutting tools and cutting conditions presented section 2.1. The 15-5PH bar has a diameter of 175 mm. The X-ray measurement have been performed with a XRD system provided by the PROTO company, using a MGR40 head and equipped with a 2 mm diameter collimator.

*Diffraction parameters:*

- Cr Kα Radiation with 18kV, 4mA
- λ = 0.229 nm, plane {211}
- Bragg angle 2θ : 155°
- Ω acquisition mode

*Measurement parameters:*

- 7 β-angles (from -30° to +30°) in both directions X and Y
- β Oscillations: ± 6°

*Stress calculation:*

- Elliptic treatment method
- Radio crystallographic elasticity constants: $\frac{1}{2} S_2 = 5.92 \times 10^{-6}$ MPa$^{-1}$, $S_1 = -1.28 \times 10^{-6}$ MPa$^{-1}$

In depth residual stress distribution has been investigated after successive layer removal by means of an electrochemical polishing system.

**4.2 Experimental results.** Fig. 10 present the measured residual stress profiles in the feed and cutting directions. Before comparing calculated and measured residual stress profiles, it is important to remind that the spot size of the X-ray system is a circle with a diameter of 2 mm and this way of measurement averages the residual stress values inside the circle. On the contrary, calculated profiles have shown that residual stresses are not homogeneous along the feed direction. The periodic variation corresponds to the feed and the magnitude of variation is around 150 MPa. This means that it is necessary to average the calculated residual stress values to compare with experimental values. This also induces an important loss of data. Much finer measuring system should be applied in the future in order to compare experimental and numerical results at a smaller scale.

Fig. 10 plots measured and calculated residual stress profiles. The measured curves profiles are closed to the calculated ones. The compression picks are located at the same depth. Compressive residual stress values are similar in the feed direction and in the cutting speed direction, the

difference is about 60MPa. Concerning residual stresses at the surface, its value is not stable due to the very strong gradient in the subsurface. Nevertheless, the difference between numerical and experimental values doesn't exceed 160MPa.

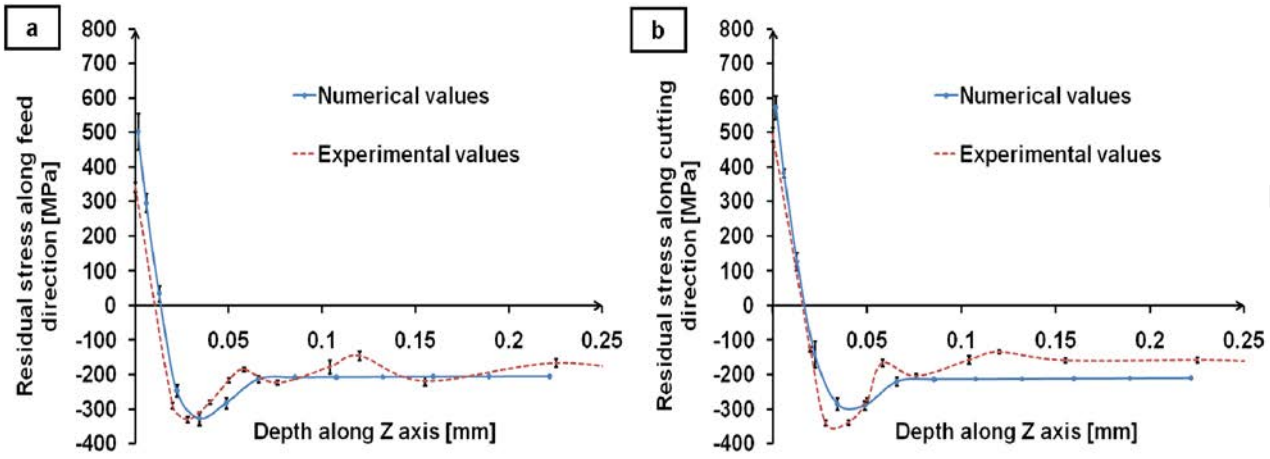


Fig. 10: Comparison of average calculated and measured residual stress profiles: (a) along the feed direction: X axis; (b) along the cutting speed direction: Y axis.

## 5. Conclusions

This article presents a method for 3D modeling of residual stresses generated by machining operations. The first part of the paper presents this new approach which consists in modeling only the action of the process on the machined surface of the workpiece. The hybrid model does not simulate the chip formation and the material separation around the cutting edge. It focuses only onto the thermo-mechanical loadings applied onto the machined surface which are responsible of the residual stresses formation. This new method applied to a 3D multipass simulation enables to model several tool passages onto the machined surface. With this method it becomes possible to estimate the number of passages leading to a steady state. The model reveals also that residual stresses are not homogenous on the external surface. The period corresponds to the feed of the cutting tool and the ± 150MPa of variation around the average value are very important. In order to compare the numerical results with experimental measurements, only the average value has been considered to obtain accurate comparison with residual stress profiles recorded with X-ray diffraction method. For both numerical and experimental results, affected zone is about 0.2mm and the external layer is in tension followed by a compression pick below the surface. To finish, calculated and measured stress values are really closed. The next step concerning the model improvement will be the consideration of change of phase during machining. This development will allow to test capacities and robustness of the model in a large range of cutting parameters (change of feed rate and cutting speed, worn tool, dry condition,…).

## 6. Acknowledgements

Authors would like to express their gratitude to the EUROCOPTER Company, AREVA NP Company and the CETIM Company for their financial support.

## 7. References


[1] H.R. Habibi Bajguirani, Materials Science and Engineering, A338 (2002), p.142-159.

[2] M. Aghaie-Khafri and F. Adhami, Materials Science and Engineering, A527, Issues 4-5 (2010), p.1052-1057.

[3] Tong Wu, in: *Experiment and numerical simulation of welding induced damage of stainless steel 15-5PH*, PhD Thesis, INSA Lyon, (2007).

[4] J. Paulo Davim, in: *Machining: fundamentals and recent advances*, edited by Springer, Vol. XIV. ISBN 978-1-84800-212-8, (2008).

[5] E. Capello, Journal of Materials Processing Technology, 160 (2005), p.221-228.

[6] E.K Henriksen, *Residual Stresses in Machined Surfaces*, Trans. ASME, 73 (1951), p.69-76.

[7] C.R. Liu and M.M. Barash, *Variables governing patterns of mechanical residual stresses in machined surfaces*, Trans. ASME, J. Eng. Ind, 104 (1982), p.257-264.

[8] D. Ulutan, B. Erdem Alaca and I. Lazoglu, Journal of Materials Processing Technology, 183 (2007), p.77-87.

[9] X. Deng and C. Shet, International Journal of Machine Tool and Technology, 43 (2007), p.573-587.

[10] M. Salio, T. Berruti and G. De Poli, International Journal of Mechanical Sciences, 48 (2006), p.976-984.

[11] E. Ceretti et al., Journal of Materials Processing Technology, 59 (1996), p.169-180.

[12] K.C. Ee, Journal of materials processing technology, 47 (2005), p.1611-1668.

[13] C.R. Liu and Y.B. Guo, International Journal of Mechanical Science, 42 (2000), p.1069-1086.

[14] Mohamed N.A. Nasr, E.-G Ng and M.A. Elbestawi, International Journal of Machine Tools and Manufacture, 47 (2007), p.401-411.

[15] F. Valiorgue, Journal of Materials Processing Technology, 191 (2007), p.270-273.

[16] H. Sasahara, T. Obikawa and T. Shirakashi, International Journal of Machine Tools and Manufacture, 44 (2004), p.815-822.

[17] A. Attanasio, E. Ceretti and C. Giardini, Machining Science and Technology, 13 (2009), p.317-337.

[18] Frédéric Valiorgue, Joël Rech, Hédi Hamdi, Philippe Gilles and Jean-Michel Bergheau: submitted in International Journal of Mechanical Sciences (2011).

[19] C. Bonnet, F. Valiorgue, J. Rech, C. Claudin, H. Hamdi, J.M. Bergheau and P. Gilles, International Journal of Machine Tools and Manufacture, 48 (2008), p.1211-1223.

[20] J.Iraola, MSc student, final project, ENISE (France) & Univ. Mondragon (Spain), (2010).

[21] Xiaoping Li, Journal of Materials Processing Technology, 62 (1996), p.149-15.